Solution Structure of the Quaternary MutT−M^{2+}−AMPCPP−M^{2+} Complex and Mechanism of Its Pyrophosphohydrolase Action[†,‡]

Jian Lin,[§] Chitrananda Abeygunawardana,[§] David N. Frick,[||,⊥] Maurice J. Bessman,[||] and Albert S. Mildvan*[,§]

Department of Biological Chemistry, The Johns Hopkins School of Medicine, 725 North Wolfe Street, Baltimore, Maryland 21205-2185, and Department of Biology, The Johns Hopkins University, Charles and 34th Streets, Baltimore, Maryland 21218

Received October 18, 1996; Revised Manuscript Received December 4, 1996[⊗]

ABSTRACT: The MutT enzyme (129 residues) catalyzes the hydrolysis of nucleoside triphosphates (NTP) by substitution at the rarely attacked β-P, to yield NMP and pyrophosphate. It requires two divalent cations, forming an active E−M^{2+}−NTP−M^{2+} complex. The solution structure of the free enzyme consists of a five-stranded mixed β-sheet connected by loop I−α-helix I−loop II, by two tight turns, and by loop III and terminated by loop IV−α-helix II [Abeygunawardana, C., *et al*. (1995) *Biochemistry 34*, 14997−15005]. Assignments of backbone ^{15}N and NH resonances and side chain ^{15}N and NH_2 resonances of the quaternary complex were made by $^1H-^{15}N$ HSQC titrations of the free enzyme with $MgCl_2$ followed by equimolar AMPCPP/$MgCl_2$. H_α assignments were made by $^1H-^{15}N$ 3D TOCSY HSQC, and $^1H-^{13}C$ CT-HSQC spectra and backbone and side chain ^1H and ^{13}C assignments were made by 3D HCCH TOCSY experiments. Ligands donated by the protein to the enzyme-bound divalent cation, identified by paramagnetic effects of Co^{2+} and Mn^{2+} on CO(C)H spectra, are the carboxylate groups of Glu-56, -57, and -98 and the amide carbonyl of Gly-38. The solution structure of the complex was computed with XPLOR using a total of 2168 NOE and 83 ϕ restraints for the protein, 11 intramolecular NOEs for bound Mg^{2+}AMPCPP, 22 intermolecular NOEs between MutT and AMPCPP, and distances from the enzyme-bound Co^{2+} to the three phosphorus atoms of $Co^{3+}(NH_3)_4$AMPCPP from paramagnetic effects of Co^{2+} on their T_1 values. The fold of the MutT enzyme in the complex is very similar to that of the free enzyme, with minor changes in the metal and substrate binding sites. The adenine ring binds in a hydrophobic cleft, interacting with Leu-4 and Ile-6 on β-strand A and with Ile-80 on β-strand D. The 6-NH_2 group of adenine approaches the side chain NH_2 of Asn-119. This unfavorable interaction is consistent with the stronger binding by MutT of guanine nucleotides, which have a 6-keto group. The ribose binds with its hydroxyl groups oriented toward the solvent and its hydrophobic face interacting with Leu-4, Ile-6, and the γ-CH_2 of Lys-39 of loop I. The metal−triphosphate moiety appears to bind in the second coordination sphere of the enzyme-bound divalent cation. One of two intervening water ligands is well positioned to attack P_β with inversion and to donate a hydrogen bond to the conserved residue, Glu-53, which may deprotonate or orient the attacking water ligand. Lys-39 which is positioned to interact electrostatically with the α-phosphoryl group may facilitate the departure of the leaving NMP. On the basis of the structure of the quaternary complex, a mechanism of the MutT reaction is proposed which is qualitatively and quantitatively consistent with kinetic and mutagenesis studies. It is suggested that similar mechanisms may be operative for other enzymes that catalyze substitution at P_β of NTP substrates.

The MutT enzyme, a pyrophosphohydrolase of 129 residues, catalyzes the unusual hydrolysis of nucleoside and deoxynucleoside triphosphates (NTP) by nucleophilic substitution at the rarely attacked β-phosphorus, yielding pyrophosphate and a nucleotide (NMP) as products (Bhatnagar *et al*., 1991; Weber *et al*., 1992a). Like other enzymes which catalyze substitution at the electron-rich β-phosphorus, this enzyme requires two divalent cations for activity (Frick *et al*., 1994). The biological role of this enzyme is to prevent AT → CG transversions (Yanofsky *et al*., 1966) by preferentially hydrolyzing a mutagenic form of dGTP which mispairs with template A, thus "sanitizing" the nucleotide pool (Bhatnagar *et al*., 1991, and references therein). Maki and Sekiguchi (1992) have proposed that the biological substrate of the MutT enzyme is 8-oxo-dGTP, an oxidatively modified nucleotide which can mispair with template adenine during DNA synthesis *in vitro* (Cheng *et al*., 1991), and have characterized a similar enzyme from a human cell line (Mo *et al*., 1992; Sakumi *et al*., 1993) and from mice (Kakuma *et al*., 1995). The MutT enzyme is part of a larger family of sequence-related phosphohydrolases which appear to serve a "housecleaning" function in cells (Bessman *et al*., 1996).

[†] This work was supported in part by National Institutes of Health Grants DK28616 (to A.S.M.) and GM18649 (to M.J.B.). J.L. is a Postdoctoral Fellow of the American Cancer Society.

[‡] A complete listing of the distance restraints derived from NOE data has been deposited at the Brookhaven Protein Data Bank (Chemistry Department, Brookhaven National Laboratory, Upton, NY) (file name R1TUMMR) together with the atomic coordinates of the family of 16 acceptable structures (file name 1TUM).

* To whom correspondence should be addressed. Phone: 410-955-2038. Fax: 410-955-5759.

[§] The Johns Hopkins School of Medicine.

[||] The Johns Hopkins University.

[⊥] Present address: Department of Biological Chemistry and Molecular Pharmacology, Harvard Medical School, 240 Longwood Ave., Boston, MA 02115.

[⊗] Abstract published in *Advance ACS Abstracts,* February 1, 1997.

S0006-2960(96)02619-0 CCC: $14.00

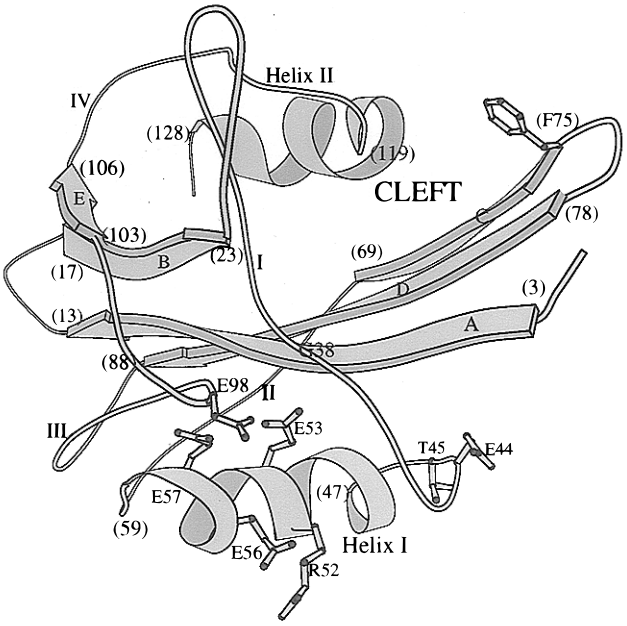

FIGURE 1: Solution structure of the free MutT enzyme (Abeygunawardana *et al*., 1995) showing the conserved residues and the secondary structural components. Numbers in parentheses indicate residues at the beginnings and ends of the secondary structural components. This lowest-energy structure, drawn with MOLSCRIPT (Kraulis, 1991), shows C_α connectivities. Due to few NOE restraints, the side chain conformations of E44, E56, and E98 are not well-defined.

Heteronuclear NMR[1] studies of MutT have shown the solution secondary structure to consist of a five-stranded mixed β-sheet connected by the loop I−α-helix I−loop II motif, by two tight turns, and by loop III and terminated by loop IV−α-helix II (Abeygunawardana *et al*., 1993; Weber *et al*., 1993). The tertiary structure (Figure 1, Abeygunawardana *et al*., 1995) is globular and compact, with the parallel portion of the β-sheet sandwiched between the two α-helices, forming an α+β-fold. A cluster of four conserved glutamate residues (53, 56, 57, and 98) form a patch of strongly negative electrostatic potential in the three-dimensional structure.

Previous mutagenesis and structural studies have shown that Glu-57 provides one of the ligands to the enzyme-bound divalent cation (Lin *et al*., 1996). Other possible ligands, suggested by the proximity of the enzyme-bound metal to their backbone NH groups, include the carboxylate side chains of Glu-53, Glu-56, and Glu-98 and the amide carbonyl groups of Gly-38 and Lys-39. Nucleotide binding altered backbone ^{15}N and NH chemical shifts along β-strands A, C, and D of the β-sheet and at the beginning of helix II, suggesting that the cleft region (Figure 1) contributes to the substrate binding site.

To clarify these points, and to learn in detail the sites of interaction of the essential divalent cation and the metal−NTP substrate with the enzyme, we have determined the solution structure of the quaternary MutT−M^{2+}−AMPCPP−M^{2+} complex, using AMPCPP which was previously shown to be a nonhydrolyzable substrate analog for MutT (Frick *et al*., 1994; Lin *et al*., 1996). The structure of the quaternary complex leads directly to a reasonable and testable mechanism of the MutT reaction which may also apply to other enzymes that catalyze nucleophilic substitution at P_β of NTP substrates.

MATERIALS AND METHODS

Materials. Uniformly isotopically enriched compounds, including $^{15}NH_4Cl$ (99% ^{15}N), D_2O (99.996% ^2H), and glucose (99% ^{13}C), were purchased from Cambridge Isotope Labs (Woburn, MA). AMPCPP was purchased from Sigma. The MutT enzyme, labeled with ^{13}C and/or ^{15}N, was isolated and purified as previously described (Abeygunawardana *et al*., 1993) and was assayed with dGTP as substrate, as previously described (Frick *et al*., 1994).

The sample conditions for the NMR studies of the MutT−Mg^{2+}−AMPCPP−Mg^{2+} complex were 0.75 mM labeled MutT, 10 mM Tris-HCl (pH 7.5), 16 mM $MgCl_2$, and 8 mM AMPCPP, in H_2O/D_2O (90:10) for the ^{15}N-labeled protein or in D_2O for the $^{13}C/^{15}N$-labeled protein.

NMR Spectroscopy. Unless otherwise noted, NMR experiments were performed on a Varian Unityplus 600 spectrometer equipped with four independent RF channels and Z gradient capabilities at 32 °C using the Nalorac 8 mm triple-resonance, pulsed field gradient probe and a 22 mm sample column (850 μL) in Shigemi 8 mm NMR tubes. All multidimensional data sets were recorded using the States−TPPI method (Marion *et al*., 1989) in all indirect dimensions, with a relaxation delay of 1.0−2.0 s. In some NMR experiments, the original pulse sequences were modified to include gradient pulses and water flip-back pulses in order to minimize artifacts and to avoid saturation of the water resonances (Table 1).

NMR experiments used for protein resonance assignments, *i.e*. 2D $^1H-^{13}C$ CT-HSQC and 3D HCCH-TOCSY experiments, as well as for intramolecular NOE studies, *i.e*. 3D $^1H-^{15}N$ NOESY-HSQC and 3D $^1H-^{13}C$ NOESY-HSQC spectra, were acquired as described previously for the free enzyme, and the parameters are given in Table 1 (Abeygunawardana *et al*., 1995).

3D COCH experiments, which correlate side chain carbonyl carbon resonances ($^{13}C_i{=}O$) with $^{13}C_{i-1}$ and $^{13}C_{i-2}$ resonances and those of protons attached to the C_{i-1} carbon, were acquired with the pulse sequence of Kay (1993). All ^{13}C pulses were applied at 43 ppm, and the refocusing delay, τ_d, was set to 0.9 ms to optimize correlations for side chain methylene groups. All other parameters were as described (Kay, 1993) (Table 1).

Intermolecular NOEs between protons of AMPCPP and those of the $^{13}C/^{15}N$-labeled MutT enzyme in D_2O were acquired using the ^{13}C-filtered NOESY-HMQC sequence of Lee *et al*. (1994) with mixing times of 400 ms and 1 s. To improve the sensitivity, experiments were carried out as two sets of 2D spectra, rather than as one 3D experiment, with frequency labeling of either ^{13}C-bound proton resonances or the attached ^{13}C resonances of the enzyme (Table 1). The long mixing times were necessary to accumulate sufficient signal, because the binding of AMPCPP to the MutT enzyme

[1] Abbreviations: AMPCPP, α,β-methyleneadenosine triphosphate; CT, constant time; DGSA, distance geometry-simulated annealing; HMQC, heteronuclear multiple-quantum correlation; HSQC, heteronuclear single-quantum correlation; NMR, nuclear magnetic resonance; NOE, nuclear Overhauser effect; NOESY, nuclear Overhauser effect spectroscopy; 2D, two-dimensional; 3D, three-dimensional; RF, radiofrequency; TES, *N*-[tris(hydroxymethyl)methyl]-2-aminoethanesulfonic acid; TOCSY, total correlation spectroscopy; TPPI, time-proportional phase incrementation; TSP, sodium 3-(trimethylsilyl)-propionate-2,2,3,3-d_4.

Table 1: Acquisition and Processing Parameters of the NMR Experiments Used in the Study of the MutT−M^{2+}−AMPCPP−M^{2+} Complex

experiment	pulse sequence	isotope label	dimension	sweep width (Hz)	center (ppm)	acquisition time (ms)	complex points	mixing time (ms)	scans per FID	total time (h)	data matrix (points)	digital resolution (ppm/point)
(1) ^{1}H−^{15}N HSQC	*a*	^{15}N	^{15}N (t_1)	1946	121.0	131.5	256	−	4	0.8	1024	0.031
			NH (t_2)	8000	4.71	128.0	1024				1024	0.005
(2) 3D TOCSY-HSQC	*b*	^{15}N	^{1}H (t_1)	7200	4.71	12.8	92	32	8	30	512	0.023
			^{15}N (t_2)	1900	121.0	16.8	32				128	0.24
			NH (t_3)	10000	4.71	64.0	640				512	0.010
(3) 3D NOESY-HSQC	*c*	^{15}N	^{1}H (t_1)	7200	4.71	17.8	128	100	4	22	512	0.023
			^{15}N (t_2)	1900	121.0	16.8	32				128	0.24
			NH (t_3)	8000	4.71	64.0	512				512	0.010
(4) 3D HMQC-J	*d*	^{15}N	^{15}N (t_1)	1900	121.0	404.0	768	−	16	14	8192	0.004
			NH (t_2)	8000	4.71	64.0	512				1024	0.005
(5) 2D ^{1}H−^{13}C CT-HSQC	*e*	^{13}C/^{15}N	^{13}C (t_1)	9052	43.0	21.7	196	−	16	16	2048	0.030
		(in D_2O)	^{1}H (t_2)	10000	4.71	58.0	576				2048	0.004
(6) 3D HCCH-TOCSY	*f*	^{13}C/^{15}N	^{1}H (t_1)	4200	3.00	22.9	96	17.8	8	30	512	0.014
		(in D_2O)	^{13}C (t_2)	4525	43.0	7.1	32				128	0.23
			^{1}H (t_3)	8400	3.00	61.0	512				512	0.014
(7) 3D NOESY-HSQC	*g*	^{13}C/^{15}N	^{1}H (t_1)	5280	3.63	22.0	116	100	8	51	512	0.017
		(in D_2O)	^{13}C (t_2)	4525	43.0	9.3	42				128	0.23
			^{1}H (t_3)	8000	3.63	64.0	512				512	0.013
(8a) 2D NOESY-HMQC	*h*	^{13}C/^{15}N	^{1}H (t_1)	6000	4.71	21.3	128	1000	96	23	512	0.020
		(in D_2O)				18.3	110	400	256	42		
			^{13}C		43.0							
			^{1}H (t_2)	8000	4.71	128.0	1024				2048	0.007
(8b) 2D NOESY-HMQC	*h*	^{13}C/^{15}N	^{13}C (t_1)	9050	43.0	6.0	54	1000	256	25	256	0.230
		(in D_2O)	^{1}H (t_2)	8000	4.71	128.0	1024				2048	0.007
(9) 3D COCH	*i*	^{13}C/^{15}N	^{13}C (t_1)	3016	43.0	6.6	20	−	32	71	256	0.078
		(in D_2O)	^{13}C (t_2)	832	43.0	76.9	64				128	0.043
			^{1}H (t_3)	7200	4.71	71.0	512				256	0.006
(10a) 2D CO(C)H	*i*	^{13}C/^{15}N	^{13}C (t_1)	2242	43.0	57.1	128	−	16	2 × 5	512	0.030
Co^{2+} titration		(in D_2O)	^{1}H (t_2)	7200	4.71	71.0	512				1024	0.006
(10b) 2D CO(C)H	*i*	^{13}C/^{15}N	^{13}C (t_1)	1601	43.0	100.0	160	−	16	1.25 × 6	1024	0.010
Mn^{2+} titration		(in D_2O)	^{1}H (t_2)	7200	4.71	71.0	512				1024	0.006

[a] Bodenhausen and Ruben (1980) and Mori *et al*. (1995). [b] Marion *et al*. (1989). [c] Marion *et al*. (1989) and Abeygunawardana *et al*. (1996). [d] Kay and Bax (1990). [e] Vuister and Bax (1992). [f] Bax *et al*. (1990) and Kay *et al*. (1993). [g] Muhandiram *et al*. (1993). [h] Lee *et al*. (1994). [i] Kay (1993).

is weak; K_D (E−Mg^{2+}−AMPCPP−Mg^{2+}) = 0.28 mM (Frick *et al*., 1994), and shorter mixing times did not provide enough sensitivity, as observed with other systems (Lee *et al*., 1995, and references therein).

Co^{2+} and Mn^{2+} Titrations of the MutT Enzyme. To determine the ligands of the enzyme-bound divalent cation, 2D CO(C)H experiments were recorded using the pulse sequence described above (Table 1) with 0.75 mM $^{13}C/^{15}N$-labeled MutT enzyme, 10 mM TES buffer (in the $CoCl_2$ titrations), or 10 mM Tris buffer (in the $MnCl_2$ titrations) (pH 7.5) in D_2O (without AMPCPP and $MgCl_2$) in the presence of either 0, 5, 10, 15, 25, and 35 μM $CoCl_2$ or 0, 0.3, 0.6, 0.9, 1.2, and 1.5 μM $MnCl_2$. Data were collected using samples volumes of 0.65 mL in a 5 mm triple-resonance, pulsed field gradient probe. All data sets were processed on Silicon Graphics workstations (Indigo^{2}XZ or Personal IRIS 4D/35) using the FELIX software package (Biosym Technologies, Inc.). The observed ^1H chemical shifts are reported with respect to the H_2O or HOD signal, which is taken as 4.706 ppm downfield from external TSP at 32 °C. The carbon chemical shifts are reported with respect to external TSP in D_2O (0.0 ppm). The nitrogen chemical shifts are reported with respect to external $^{15}NH_4Cl$ (2.9 mM in 1 M HCl) at 20 °C, which is 24.93 ppm downfield from liquid NH_3 (Levy & Lichter, 1979). The phosphorus chemical shifts are reported with respect to 85% H_3PO_4 containing 20% D_2O.

Paramagnetic Effects of Enzyme-Bound Co^{2+} on the Phosphorus Atoms of AMPCPP in the Quaternary MutT−Co^{2+}−AMPCPP−$Co^{3+}(NH_3)_4$ Complex. To ensure the binding of paramagnetic Co^{2+} *only* to the enzyme site, and not to the nucleotide site, the substitution-inert, diamagnetic, stable complex, β,γ-bidentate $Co^{3+}(NH_3)_4$AMPCPP, was used in place of MgAMPCPP. It was prepared, purified, and characterized by ^{31}P NMR as previously described (Cornelius *et al*., 1977; Cleland & Mildvan, 1979; Granot *et al*., 1980b).

A solution containing 0.5 mM MutT, 2.40 mM $Co^{3+}(NH_3)_4$-AMPCPP, 1.3 mM Tris-HCl-d_{11} buffer (pH 7.5), and 10% D_2O in a total volume of 2.0 mL at 20 °C was titrated with $CoCl_2$ at concentrations of 0, 24, 73, 147, 220, and 293 μM, monitoring the longitudual relaxation rates ($1/T_1$) of the ^{31}P resonances of $Co^{3+}(NH_3)_4$AMPCPP at 242.9 MHz with a Bruker AM 600 NMR spectrometer, equipped with a 10 mm broad band probe. To minimize the recycle time, the nonselective saturation−recovery method, with 8−10 relaxation delays, was used to measure T_1, as previously described (Serpersu *et al*., 1988; Weber *et al*., 1991). For each spectrum, 16K data points were collected over a spectral width of 10 000 Hz with an acquisition time of 0.8192 s. Four scans per spectrum were generally sufficient to obtain adequate signal:noise, *i.e*. >10:1. To permit calculation of the correlation time for dipolar interaction, the T_1 values were also measured at 101.3 MHz on selected samples from the titration, at $CoCl_2$ concentrations of 0, 73, and 293 μM, using a Bruker AM 250 NMR spectrometer. For each spectrum, 4K data points were collected over a spectral width of 5000 Hz with an acquisition time of 0.4096 s. Depending on the concentration of $CoCl_2$, 128−1024 scans per spectrum were required to obtain adequate signal:noise. Conditions were otherwise as described at 242.9 MHz.

The data were analyzed as previously described (Serpersu *et al*., 1988) by plotting the increase in $1/T_1$ for each ^{31}P resonance as a function of the total concentration of added Co^{2+}. The slopes of these linear plots, when multiplied by the total concentration of $Co^{3+}(NH_3)_4$AMPCPP, yielded $1/fT_{1P}$, the normalized longitudual relaxation rates. These values were then corrected for the fraction of Co^{2+} which was present in the quaternary complex, estimated as 38% from a consideration of the distribution of Co^{2+} among three forms: the free ion, the binary MutT−Co^{2+}, and the quaternary MutT−Co^{2+}−AMPCPP−$Co^{3+}(NH_3)_4$ complexes. This distribution was calculated from the dissociation constant of Co^{2+} from the quaternary complex of 25 ± 9 μM as determined by competition with Mn^{2+} binding which was monitored by EPR and by $1/T_{1P}$ of water protons at 24.3 MHz, as previously described (Serpersu *et al*., 1988; Weber *et al*., 1991), and from the K_I of $Co(NH_3)_4$AMPCPP in the Co^{2+}-activated MutT reaction of 3.7 mM, as determined by standard kinetic assays in competition with Mg^{2+}dGTP (Frick *et al*., 1994). The corrected values of $1/fT_{1P}$ were then used, with the dipolar term of the Solomon−Bloembergen equation, to calculate $Co^{2+}-{}^{31}P$ distances in the quaternary complex, as previously described (Mildvan & Gupta, 1978; Serpersu *et al*., 1988; Weber *et al*., 1991).

Structural Calculations. The NOE cross-peak intensities were classified as strong, medium, and weak and assigned distance restraints of 1.8−2.8, 1.8−3.2, and 1.8−5.0 Å, respectively (Clore *et al*., 1986). Pseudoatom corrections were added to the upper limit for constraints involving NOEs to methyl protons (1.0 Å), to nonstereospecifically assigned methylene protons (1.0 Å), to degenerate methyl protons of Leu and Val residues (1.7 Å), and to δ and ϵ protons of Tyr and Phe residues (2.3 Å) (Wüthrich *et al*., 1983; Wüthrich, 1986; Clore *et al*., 1987). Using $^1H-{}^{13}C$ NOESY-HSQC data, an additional 0.5 Å was added for NOEs involving methyl protons to account for their higher apparent intensities, resulting from slower relaxation. Only structurally useful intraresidue NOEs were included in the interproton distance restraints. Thus, NOEs between geminal protons or between vicinal methylene protons were not used. $^3J_{NH-H\alpha}$ values were interpreted and incorporated as torsional angle (ϕ) restraints where $\phi = -60 \pm 20°$ for $^3J_{NH-H\alpha} < 6.0$ Hz and $\phi = -120 \pm 40°$ for $^3J_{NH-H\alpha} \geq 7.5$ Hz. A total of 83 ϕ dihedral angle restraints from $^3J_{NH-H\alpha}$ coupling constant measurements were used with a force constant of 200 kcal mol^{-1} rad^{-2}.

The structures of the quaternary MutT−M^{2+}−AMPCPP−M^{2+} complex were calculated from randomized initial structures using the hybrid distance geometry-simulated annealing (DGSA) protocol (Nilges *et al*., 1988) in the program XPLOR 3.1 (Brünger, 1992) on a Convex C220 computer. A total of 2168 intramolecular and 22 intermolecular NOE-derived distance restraints were applied to the MutT enzyme and between the enzyme and AMPCPP, respectively. The conformation of AMPCPP in the complex was determined by using 11 intramolecular distance restraints and two dihedral angle restraints previously reported (Frick *et al*., 1995) using the error limits in the distances as the upper and lower limits for the restraints. The nucleotide-bound metal was chelated by oxygen atoms of the β- and γ-phosphates of AMPCPP in the Λ configuration as previously determined (Frick *et al*., 1994). The enzyme-bound metal was restrained by four metal ligands from oxygen atoms of the side chain carboxylates of Glu-56, Glu-57, and Glu-98 and the backbone carbonyl oxygen of Gly-38, as

found experimentally (see below), with a lower limit of 2.0 Å and an upper limit of 2.4 Å. In addition, two water ligands to the enzyme-bound metal with distance restraints of 2.0−2.4 Å were incorporated into the structure, on the basis of previous water relaxation studies with enzyme-bound Mn^{2+} (Frick *et al*., 1994; Lin *et al*., 1996). Distance restraints from the enzyme-bound metal to the three phosphorus atoms of AMPCPP were based on their experimental measurement by paramagnetic effects of enzyme-bound Co^{2+} on the $1/T_1$ values of each phosphorus of β,γ-bidentate $Co^{3+}(NH_3)_4$-AMPCPP, a diamagnetic, substitution-inert, stable analog of Mg^{2+}−AMPCPP.

The structural calculations were made using a square-well potential and a force constant of 50 kcal mol^{-1} $Å^{-2}$. Using these restraints, a total of 40 structures were generated by the DGSA protocol. These 40 structures were then subjected to two rounds of refinement which yielded an ensemble of 16 energy-minimized structures which satisfied the criteria of no NOE violations of >0.5 Å and no dihedral violations of >5°. These 16 structures were used to define the tertiary structure of the MutT−Mg^{2+}−AMPCPP−Mg^{2+} complex.

RESULTS AND DISCUSSION

Backbone Chemical Shift Changes in the MutT−Mg^{2+}−AMPCPP−Mg^{2+} Complex. It was previously shown (Lin *et al*., 1996) that the binding of Mg^{2+} to MutT caused numerous changes in chemical shifts of backbone ^{15}N and NH resonances of the enzyme along β-strand A, β-strand B, loop I (near Gly-38), helix I (near Glu-57), and loop III (near Glu-98). Additional chemical shift changes were observed upon the subsequent binding of Mg^{2+}AMPCPP, especially along loop I. Because of these numerous changes, it was necessary to reassign the backbone and side chain chemical shifts in the MutT−Mg^{2+}−AMPCPP−Mg^{2+} complex, to collect and interpret new NOE data, and to determine the solution structure of the MutT protein in the quaternary complex. The assignments of the backbone ^{15}N and NH resonances were made by titration of the MutT enzyme with Mg^{2+} and then with AMPCPP−Mg^{2+}, closely monitoring the changes in the $^1H-^{15}N$ HSQC spectra. The assignments of most of the side chain ^1H and ^{13}C resonances were made by 2D CT-HSQC and 3D HCCH TOCSY spectra and confirmed by 3D $^1H-^{13}C$ NOESY-HSQC experiments. The chemical shift assignments of MutT in the complex are given in the Supporting Information (Table 1S).

The binding of Mg^{2+} and MgAMPCPP to the MutT enzyme to form the quaternary complex produced significant changes in chemical shifts of backbone C_α and H_α resonances along helix I, β-strands A, C, and D, and loops I and III (Figure 1). The locations of these changes are consistent with those of backbone ^{15}N and NH chemical shifts of MutT previously found on Mg^{2+} and nucleotide binding (Lin *et al*., 1996). These results suggest that the enzyme-bound metal binds near the conserved cluster of Glu residues in helix I, loop I, and loop III and that the metal nucleotide binds in the cleft between β-strands A, C, and D and helix II (Figure 1).

Determination of the Ligands of the Enzyme-Bound Metal by 2D CO(C)H Titration with $CoCl_2$ and $MnCl_2$. The MutT enzyme has been shown to be activated by Mg^{2+} or Mn^{2+}, with both ions forming an active quaternary E−M^{2+}−NTP−M^{2+} complex (Frick *et al*., 1994). Co^{2+} is also found to be an effective activator of MutT. The k_{cat} values are 3.96, 0.75, and 0.19 s^{-1} for Mg^{2+}, Co^{2+}, and Mn^{2+}, respectively.

All side chain carboxylate resonances except that of Glu-53 (see below) were assigned from 3D COCH spectra (Kay, 1993) (Table 2S). To identify the ligands of the enzyme-bound metal, distance-dependent paramagnetic effects of Co^{2+} and Mn^{2+} on side chain carboxylate resonances and backbone carbonyl resonances of MutT were monitored by 2D CO(C)H spectra. These spectra correlate the chemical shifts of all carboxylate and carbonyl carbons with those of adjacent methylene or methine protons. The glutamate region of this spectrum which correlates the δ-carboxylate carbon with the γ-methylene protons revealed pairs of signals from each glutamate residue (Figure 2A) except for Glu-53, which remains undetected over the temperature range of 14−41 °C and the pH range of 7.6−9.5. Correlation peaks for the δ-carboxylate carbon of Glu-53 were also not observed in the quaternary MutT− Mg^{2+}−AMPCPP−Mg^{2+} complex (data not shown). All resonances of Glu-53 other than that of the δ-carboxylate carbon have previously been assigned in the free enzyme (Abeygunawardana *et al*., 1995) and have been reassigned in the MutT−Mg^{2+}−AMPCPP−Mg^{2+} complex (Table 1S). The failure to detect correlations involving the δ-carboxylate, together with weaker correlations observed for the other side chain resonances of Glu-53, especially those involving the γ-methylene, suggest conformational heterogeneity of the side chain of this residue.

Titration of 750 μM MutT with $CoCl_2$ resulted in the attenuation of several carboxylate resonances, most notably those of Glu-56 and Glu-57 which become undetectable at a substoichiometric level of $CoCl_2$ (25 μM) (Figure 2B) and Glu-98 which decreased to 43% of its initial intensity at 25 μM $CoCl_2$ (panels B and C of Figure 2). These losses of signal intensity result from paramagnetic effects on $1/T_2$, broadening the resonances in both the carbon and proton dimensions, and from paramagnetic effects on $1/T_1$ which decouple the carbon from the proton signals (Villafranca & Mildvan, 1972). Under conditions of fast exchange, as established by the complete loss of signal intensities at substoichiometric levels of Co^{2+}, these paramagnetic effects on relaxation are dominated by dipolar effects which are inversely related to r^6, where r is the distance from Co^{2+} to the observed carbon and protons (Mildvan & Gupta, 1978).

For quantitative comparisons of these paramagnetic effects, $[Co^{2+}]_{1/2}$ values, the concentrations of Co^{2+} which gave half-maximal attenuation of these resonances, were calculated as 13 μM for Glu-56 and Glu-57 and 22 μM for Glu-98 (Figure 2C, Table 2). Comparably strong effects of Co^{2+} were detected on the amide carbonyl carbon of Gly-38 ($[Co^{2+}]_{1/2}$ = 18 μM). Significantly weaker paramagnetic effects of Co^{2+} occurred on the resonances of Glu-41 ($[Co^{2+}]_{1/2}$ = 36 μM) and Glu-44 ($[Co^{2+}]_{1/2}$ = 90 μM), indicating greater distances of these residues from the enzyme-bound metal ion (panels B and C of Figure 2, Table 2). No other side chain carboxylates of Glu or Asp residues or carbonyl groups of Gln or Asn residues were significantly affected by Co^{2+}. Because of the approximate linearity of these paramagnetic effects with $[Co^{2+}]$ (Figure 2C), and the essentially complete attenuation of all of the affected cross-peaks at saturating Co^{2+} concentrations, analysis of the initial slopes of these titration curves would yield the same relative distances as $[Co^{2+}]_{1/2}$.

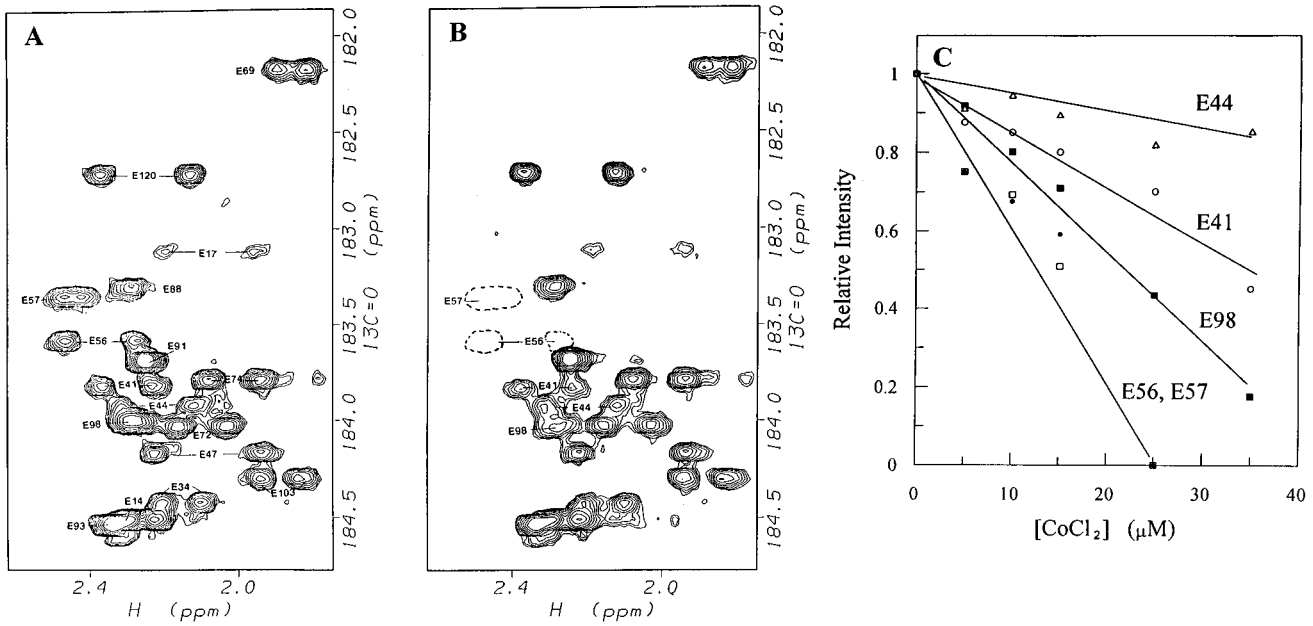

FIGURE 2: 2D CO(C)H titration of $^{15}N/^{13}C$-labeled MutT enzyme (750 μM) with $CoCl_2$. (A) Region of the CO(C)H spectrum of the MutT enzyme showing the resonances of carboxylate side chains of Glu residues. (B) Effect of 25 μM Co^{2+} on the resonances of Glu residues in the CO(C)H spectra. (C) Major effects of Co^{2+} concentration on the intensities of the side chain carboxylate resonances of Glu residues. [E41 (○), E44 (△), E56 (●), E57 (□), E98 (■)].

Table 2: Paramagnetic Effects of Co^{2+} and Mn^{2+} on Heteronuclear Resonances of MutT[a]

resonance	δ ($^1H/^{13}C$)[b] (ppm)	$[Co^{2+}]_{1/2}$ (μM)	$[Mn^{2+}]_{1/2}$ (μM)	$[Co^{2+}]_{1/2}/[Mn^{2+}]_{1/2}$
	Side Chain Carboxylate			
E56	2.47,2.27/183.58	13	0.34	38
E57	2.47,2.42/183.35	13	0.34	38
E98	2.29,2.28/184.00	22	0.65	34
E41	2.37,2.23/183.82	36	1.92	19
E44	2.31,2.12/183.92	90	5.76	16
	Backbone Carbonyl			
G37	4.69,3.89/127.39	31	1.10	28
G38	4.11/171.79	18	0.58	31
K39	4.45/175.44	27	1.02	27
	Backbone NHδ			
resonance	δ ($^1H/^{15}N$)[c] (ppm)	$[Co^{2+}]_{1/2}$ (μM)	$[Mn^{2+}]_{1/2}$ (μM)	$[Co^{2+}]_{1/2}/[Mn^{2+}]_{1/2}$
G37	8.17/109.45	ND[d]	5.25[e]	
G38	8.52/106.92	ND[d]	2.80[e]	
K39	8.37/121.94	ND[d]	2.30[e]	

[a] Effects are expressed as the metal ion concentration which halves the intensity of the indicated signal, as determined by volume integration. [b] $^1HCC{=}O$ and $^{13}C{=}O$ chemical shifts. [c] ^1HN and ^{15}N chemical shifts. [d] ND, not determined. [e] From Lin *et al*. (1996).

The absolute effects of $MnCl_2$ on 2D CO(C)H spectra of 750 μM MutT were greater than those of $CoCl_2$ by more than 1 order of magnitude, although the relative effects of Mn^{2+} on individual resonances paralleled those of Co^{2+} (Table 2). As with Co^{2+}, no other side chain carboxylates of Glu or Asp residues or carbonyl groups of Gln or Asn residues were significantly affected by Mn^{2+}. The larger absolute effects of Mn^{2+} on ^{13}C and ^1H relaxation rates (Table 2) are due to its greater effective magnetic moment resulting from the fact that Mn^{2+} has five unpaired electrons while Co^{2+} has three. Mn^{2+} also has a 10^3-fold longer electron spin relaxation time than Co^{2+} which dominates the correlation time for dipolar interaction (Mildvan & Gupta, 1978).

It has previously been shown by mutagenesis, metal binding, and $^1H-^{15}N$ HSQC titrations that Glu-57 provides a ligand to the enzyme-bound divalent cation (Lin *et al*., 1996). The large and comparable paramagnetic effects of Co^{2+} (and Mn^{2+}) on the carboxylate relaxation rates of Glu-56 and Glu-57 indicate that Glu-56 is also a metal ligand. Glu-98 which is only slightly further from the metal probably provides a third ligand. Gly-38 is a likely fourth ligand as indicated by strong paramagnetic effects of both Mn^{2+} and Co^{2+} on the carbonyl carbon relaxation rates (Table 2) and of Mn^{2+} on the $^1H-^{15}N$ relaxation rates of the adjacent amide nitrogen of Lys-39 (Table 2, Lin *et al*., 1996). Somewhat weaker effects of Mn^{2+} on the $^1H-^{15}N$ relaxation rates of Gly-38 and Gly-37 are consistent with their greater distances from the carbonyl oxygen of Gly-38. The presence of two water ligands, which would complete the octahedral coordination of the enzyme-bound divalent cation, is consistent with the 17-fold-enhanced paramagnetic effect of enzyme-bound Mn^{2+} on $1/T_1$ of water protons (Frick *et al*., 1994).

Intermolecular NOEs between AMPCPP and the MutT Enzyme in the Quaternary MutT−Mg^{2+}−AMPCPP−Mg^{2+} Complex. The conformation of Mg^{2+}AMPCPP in the quaternary complex has previously been determined as high anti-C2′exo-O1′endo, on the basis of 11 intramolecular interproton distances determined by transferred NOEs (Frick *et al*., 1995). Docking of Mg^{2+}AMPCPP into the quaternary complex required not only its conformation but also intermolecular distances from assigned proton resonances of the enzyme to those of the nucleotide. These were determined by 2D ^{13}C-filtered, isotope-edited NOESY experiments with ^{13}C-enriched MutT. Frequency labeling of the ^{13}C resonances, and of the ^{13}C-bound proton resonances, in separate 2D NOESY experiments, yielded the ^{13}C and ^1H chemical shifts of groups on the enzyme which are in close proximity to the ^{12}C-bound protons of Mg^{2+}AMPCPP. A total of 22 intermolecular NOEs from assigned proton resonances of the enzyme to those of Mg^{2+}AMPCPP were thereby obtained (Table 3).

Table 3: Intermolecular NOEs from the MutT Enzyme to Bound AMPCPP in the MutT−Mg^{2+}−AMPCPP−Mg^{2+} Complex

AMPCPP proton	MutT δ (^{1}H/^{13}C)	S:N[a]	assignment	upper limit distance[b] (Å)
AH8	1.68/46.3	3.4	L4H$\beta_{1,2}$	5.5
	1.61/28.4	2.2	L4Hγ	4.5
	0.95/25.7	5.0	L4H$\delta_{Me1,2}$	6.2
	0.46/17.8	4.4	I6Hγ_{2Me}	5.0
	1.76/42.5	2.4	I6Hβ	4.5
	0.67/12.8	2.2	I6Hδ_{Me}	5.5
AH2	1.87/42.0	2.1	I80Hβ	4.5
	1.19/28.5	3.8	I80Hγ_{11}	4.0
	1.65/28.5	3.4	I80Hγ_{12}	4.0
	0.89/14.2	9.8	I80Hδ_{Me}	5.0
AH1′	1.70/46.3	4.2	L4H$\beta_{1,2}$	6.0
	1.62/28.5	4.2	L4Hγ	4.5
	0.94/25.7	15.3	L4H$\delta_{Me1,2}$	5.2
AH2′	0.67/12.9	3.5	I6Hδ_{Me}	5.0
AH3′	0.93/25.6	3.1	L4H$\delta_{Me1,2}$	5.0
AH4′	1.68/46.4	2.4	L4H$\beta_{1,2}$	5.0
	0.94/25.8	5.2	L4H$\delta_{Me1,2}$	5.5
	1.76/29.8	2.5	K39H$\delta_{1,2}$	5.0
AH5′/5″	1.68/46.2	3.8	L4H$\beta_{1,2}$	5.5
	0.94/25.6	3.7	L4H$\delta_{Me1,2}$	6.5
$P_\alpha CH_2 P_\beta$	4.18/46.6	2.1	G38H$\alpha_{1,2}$	6.5
	1.75/29.7	2.4	K39H$\delta_{1,2}$	6.5

[a] Signal:noise, uncorrected for the number of protons involved, determined from the amplitude of the signal in the optimal slice through the cross-peak in 2D ^{13}C−^{1}H to ^{12}C−^{1}H NOESY-HMQC spectra, with a 1.0 s mixing time (Table 1, experiment 8a). [b] Upper limit used in XPLOR. The lower limit was van der Waals contact (2.0 Å).

From these NOEs, it is clear that the adenine ring binds in a hydrophobic environment near Leu-4 and Ile-6 of β-strand A and near Ile-80 of the parallel β-strand D. The ribose also interacts with Leu-4 and Ile-6 of β-strand A as well as with Lys-39 on loop I. The methylene group between P_α and P_β, corresponding to the site of bond cleavage in an NTP substrate, is near Gly-38, a likely ligand of the enzyme-bound divalent metal ion, and near Lys-39, a catalytic residue, the mutation of which to Gln results in a 42-fold decrease in k_{cat}/K_M (Frick *et al*., 1995). These intermolecular proximities are consistent with earlier phenomenological effects of NTP binding on backbone ^{15}N and NH chemical shifts (Lin *et al*., 1996) which showed changes along β-strands A, C, and D and loop I. Backbone chemical shift changes were also found on β-strand B and at the amino end of helix II possibly due to more remote effects of NTP binding on the structure of MutT.

Distances from the Enzyme-Bound Metal to the Phosphorus Atoms of the Metal−AMPCPP Complex. To position the triphosphate moiety of AMPCPP into the structure of the quaternary complex, distances from the enzyme-bound divalent cation to each of the three phosphorus atoms of the nucleotide were required. These were determined by paramagnetic effects of Co^{2+} on the $1/T_1$ values of P_α, P_β, and P_γ of the diamagnetic, substitution-inert complex, β,γ-bidentate $Co^{3+}(NH_3)_4$AMPCPP bound to MutT.

The proton-decoupled, ^{31}P NMR spectrum of uncomplexed AMPCPP at pH 7.5, 20 °C, and 242.9 MHz shows three resonances: a doublet ($^2J_{P-P}$ = 9.0 Hz) at 21.50 ppm assigned to P_α, a doublet ($^2J_{P-P}$ = 25.3 Hz) at −4.42 ppm assigned to P_γ, and a doublet of doublets ($^2J_{P-P}$ = 25.5 Hz, $^2J_{P-P}$ = 8.6 Hz) at 9.55 ppm assigned to P_β. On formation of the β,γ-bidentate $Co^{3+}(NH_3)_4$AMPCPP complex, the P_α resonance shifts upfield (by 2.85 ppm) to 18.65 ppm, the P_β resonance shifts downfield (by 18.42 ppm) to 27.97 ppm, and the P_γ resonance shifts downfield (by 9.37 ppm) to 4.95 ppm. The marked deshielding at P_β and P_γ establishes the formation of the β,γ-bidentate complex (Cornelius *et al*., 1977; Granot *et al*., 1980b).

Table 4: Distances from Co^{2+} to the Phosphorus Nuclei of AMPCPP in the MutT−Co^{2+}−AMPCPP−$Co^{3+}(NH_3)_4$ Complex

nucleus	δ[a] (ppm)	$(1/fT_{1P})_{corr}$ (242.9 MHz)[b] (s^{-1})	$(1/fT_{1P})_{corr}$ (101.3 MHz)[b] (s^{-1})	r (Co^{2+}−P)[c] (Å)
P_α	18.65	13.5 ± 1.4	16.5 ± 0.7	8.0 ± 1.7
P_β	27.97	42.0 ± 1.7	61.4 ± 6.1	6.7 ± 1.4
P_γ	4.95	56.4 ± 1.2	64.9 ± 2.6	6.3 ± 1.4

[a] ±0.05 ppm from 85% H_3PO_4 in 20% D_2O. [b] $(1/fT_{1P})_{corr}$ values were determined as described in Materials and Methods. [c] Distances were calculated with the following equations (Mildvan & Gupta, 1978; Serpersu *et al*., 1988; Weber *et al*., 1992): $(1/fT_{1P})_{corr} = q(C/r)^6 f(\tau_c)$ and $f(\tau_c) = 3\tau_c/(1 + \omega_I^2\tau_c^2) + 7\tau_c/(1 + \omega_s^2\tau_c^2)$, where q is the stoichiometric ratio of $[Co^{2+}]$ to $[Co^{3+}(NH_3)_4$AMPCPP] in the quaternary complex (q = 1 in the present case), C is a product of physical constants (C = 662 ± 93 for Co^{2+} − ^{31}P interactions), r is the metal−nucleus distance, τ_c is the dipolar correlation time (2.2 ± 0.7 ps), and ω_I and ω_S are the nuclear and electron precession frequencies, respectively. The uncertainty in the C value results from the anisotropic g value of Co^{2+} which lies in the range of 4 ± 2. Errors (∼21%) are shown in the *absolute* distances which inlcude a 14% contribution from the anisotropic g values of Co^{2+} and a ∼7% contribution from experimental errors in the measurements of $(1/fT_{1P})_{corr}$ and τ_c. The errors in the *relative* distances (∼2%) result solely from errors in $(1/fT_{1P})_{corr}$ truncated by a factor of 6 because of the r^6 relationship between $(1/fT_{1P})_{corr}$ and distance.

Titration of a solution containing MutT (0.50 mM) and $Co^{3+}(NH_3)_4$AMPCPP (2.40 mM) with $CoCl_2$, as described in Materials and Methods, resulted in a linear increase in $1/T_1$ of each of the three phosphorus resonances with increasing Co^{2+} concentration (not shown). Table 4 lists the longitudual relaxation rates, $(1/fT_{1P})_{corr}$, normalized to the concentrations of Co^{2+} and $Co^{3+}(NH_3)_4$AMPCPP and corrected for the concentration of Co^{2+} present in the quaternary MutT−Co^{2+}−AMPCPP−$Co^{3+}(NH_3)_4$ complex, at two frequencies, 242.9 and 101.3 MHz. The frequency dependencies of the $(1/fT_{1P})_{corr}$ values are consistent with them being in the fast exchange limit, permitting them to be used for distance calculations. The mean experimental ratio of [$(fT_{1P})_{corr}$ at 242.9 MHz]/[$(fT_{1P})_{corr}$ at 101.3 MHz] of 1.28 ± 0.13 (Table 4) yielded a dipolar correlation time of 2.2 ± 0.7 ps, a typical electron spin relaxation time of Co^{2+} (Serpersu *et al*., 1988; Weber *et al*., 1991). The Co^{2+}−phosphorus distances calculated from the $(1/fT_{1P})_{corr}$ values, using this correlation time, are given in Table 4. The relative distances, which are more accurate than the absolute distances because their errors result solely from the errors in $(1/fT_{1P})_{corr}$, truncated by a factor of 6 due to the sixth root taken in the calculations, indicate that the enzyme-bound Co^{2+} is closer to the β- and γ-phosphoryl groups of $Co^{3+}(NH_3)_4$AMPCPP than to the α-phosphoryl group. The absolute Co^{2+}−^{31}P distances, ranging from 6 to 8 Å, indicate that the $Co^{3+}(NH_3)_4$AMPCPP complex binds in the second coordination sphere of the enzyme-bound divalent cation, rather than in the inner sphere which would yield Co^{2+}−phosphorus distances of 3.3 Å (Serpersu *et al*., 1988).[2] An atypical location or conformation of the Co^{3+}−nucleotide complex is unlikely since $Co^{3+}(NH_3)_4$ATP is only 20-fold less active as a substrate than Mg^{2+}ATP (Frick *et al*., 1994). While an underlying inner-sphere metal−nucleotide complex

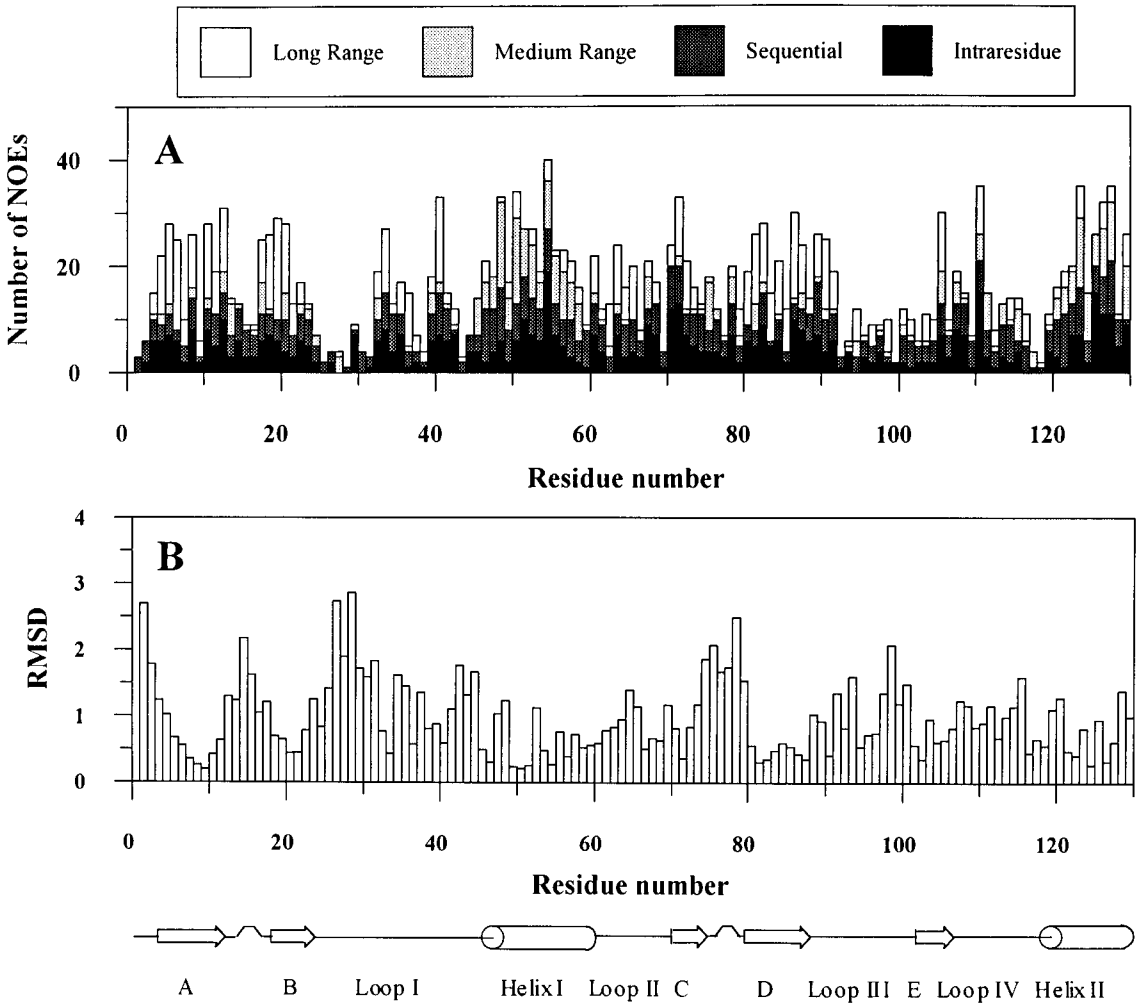

FIGURE 3: NOE distribution and rmsd values by residue of the assembled structures of the quaternary complex based on the NOE data. (A) Distribution of NOE connectivities for each residue of the MutT enzyme used to compute the solution structure of the quaternary complex. Long-range and medium-range NOEs are defined in Table 5. (B) rmsd values of all heavy atoms for each residue computed from the 16 acceptable structures of the quaternary complex.

cannot be totally excluded, it would have to exchange out of the enzyme at a rate much slower than the lowest $(1/fT_{1P})_{corr}$ value of 13.5 s^{-1} to escape detection. Such a slowly dissociating metal−NTP complex would probably not be kinetically competent to participate in catalysis by the MutT enzyme since the K_M values of Mg^{2+}dGTP and Mn^{2+}dGTP are comparable to their respective K_D values, indicating rapid pre-equilibration of these substrates with the enzyme prior to their rate-limiting hydrolysis (Frick *et al*., 1994).

Intramolecular Restraints for the Structure of the MutT Enzyme in the MutT−M^{2+}−AMPCPP−M^{2+} Complex. Intramolecular NOE restraints for the MutT enzyme in the quaternary complex were determined by 3D $^1H-^{15}N$ NOESY-HSQC and 3D $^1H-^{13}C$ NOESY-HSQC spectra. NOE peak lists were assigned on the basis of chemical shift data and converted into an XPLOR input file using an in-house-written computer program. The input file was subsequently edited manually to remove multiple possible assignments of NOEs resulting from chemical shift degeneracies. A total of 2168 intramolecular NOEs were assigned and used in the structure determination, of which 607 were long-range, 358 were medium-range, 586 were sequential, and 617 were intraresidue (Figure 3A). The NOEs were well distributed over the enzyme except for the first three residues at the N terminus, residues 25−28 of loop I, residues 92−102 of loop III, and residues 116−118 of loop IV. Also used in the structure determination were 83 ϕ dihedral angle restraints based on $^3J_{NH-H_\alpha}$ coupling constants obtained from $^1H-^{15}N$ HMQC-J experiments.

All of the intermolecular and intramolecular distance restraints and the intramolecular dihedral angle restraints were used to calculate the structure of the quaternary MutT−M^{2+}−AMPCPP−M^{2+} complex using the standard simulated annealing protocol of XPLOR 3.1. A total of 16 acceptable structures of the complex were generated which are superimposed in Figure 4, and the input data and structural statistics are summarized in Table 5. The average rmsd values of the backbone and of all heavy atoms of the protein in the complex are low, indicating a well-defined structure (Table 4). The individual rmsd values for the backbone heavy atoms as a function of residue number correlate well with the number of NOE restraints (Figure 3A,B). The conformation of the triphosphate moiety of AMPCPP is less

[2] A second solution of the relaxation equation from the ratio of relaxation rates at two frequencies of 1.28 yields a dipolar correlation time of 0.32 ps, which is unprecedentedly short for Co^{2+} complexes (Mildvan & Gupta, 1978; Serpersu *et al*., 1988; Weber *et al*., 1991) and provides an extreme lower limit. If this short correlation time were correct, the absolute Co^{2+} to phosphorus distances would be shorter by 20% which is within their experimental errors given in Table 4. Hence, the conclusion of a second sphere complex would be unchanged.

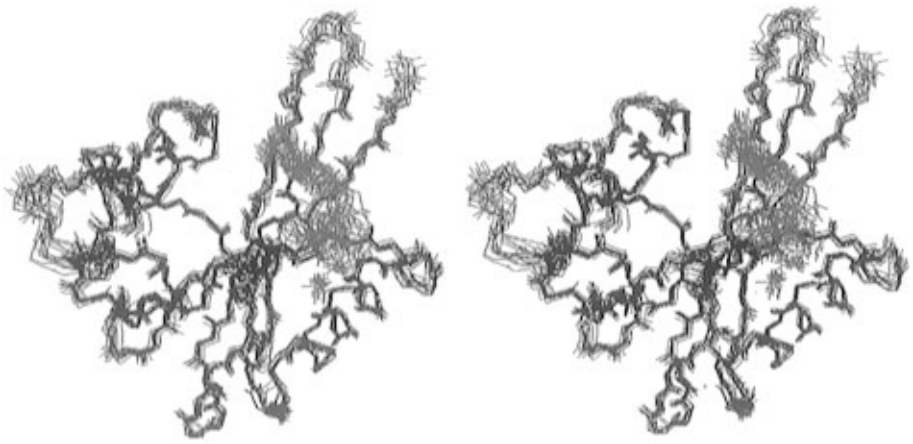

FIGURE 4: Stereopair of the superposition of the backbone (N, C_α, and CO) atoms of 16 acceptable structures of the MutT−M^{2+}−AMPCPP−M^{2+} complex. Table 5 gives the statistics of this set of structures. AMPCPP and metal ions are shown in red. Structures are drawn with INSIGHT II (Biosym Technologies, San Diego).

Table 5: NMR Restraints and Structural Statistics for the MutT−M^{2+}−AMPCPP−M^{2+} Complex

Input Restraints	
intramolecular NOEs for MutT	
long-range ($\|i-j\| > 5$) NOEs	607
medium-range ($1 < \|i-j\| \leq 5$) NOEs	358
sequential ($\|i-j\| = 1$) NOEs	586
intraresidue NOEs	617
total NOEs	2168
NOEs/residue	16.8
dihedral angles (ϕ)	83
intermolecular NOEs between AMPCPP and MutT	
total NOEs	22
intramolecular NOEs for AMPCPP	
total NOEs	11

rmsd from Idealized Geometry	best structure	average of 16 structures
bonds (Å)	0.0043	0.0043 ± 0.0002
angles (deg)	0.899	0.907 ± 0.032
impropers (deg)	0.457	0.462 ± 0.056
E_{NOE} (kcal/mol)	80.4	94.0 ± 13.6
E_{REPEL} (kcal/mol)	94.6	99.7 ± 19.7
E_{VDW} (kcal/mol)[a]	−603.8	−596.2 ± 7.6

rmsd of Ensemble of 16 Structures (Å)[b]	pairwise rmsd	rmsd from mean
backbone−secondary	0.75 ± 0.11	0.52 ± 0.09
all protein heavy atoms	1.30 ± 0.11	0.89 ± 0.15
all heavy atoms	1.32 ± 0.10	0.90 ± 0.13
all AMPCPP heavy atoms	1.76 ± 0.52	1.20 ± 0.49

[a] Calculated using 0.8 × (the CHARMM parameters) (Brooks *et al*., 1983). [b] The 16 acceptable structures were aligned on the backbone heavy atoms of all residues.

precisely defined due to the fewer distance restraints available (see below).

Structure of the MutT−M^{2+}−AMPCPP−M^{2+} Complex. Figure 4 shows a superposition of the 16 acceptable structures of the quaternary MutT−M^{2+}−AMPCPP−M^{2+} complex, and Figure 5 shows one of the two lowest-energy structures which most closely resembles the average structure. While the global fold of the MutT enzyme in the quaternary complex is very similar to that of the free enzyme, some localized structural differences were found. Thus, the mean pairwise rmsd between the free and complexed enzyme was 2.15 ± 1.16 Å for all backbone heavy atoms and 2.96 ± 1.48 Å for all heavy atoms. These values overlap with the respective sums of the rmsd values for all backbone heavy atoms, separately calculated for the free and bound enzyme (2.01 Å) and for all heavy atoms, separately calculated for the free and bound enzyme (3.50 Å) indicating that much of the calculated difference results from variation *within* the structures of the free and complexed MutT.

When this analysis was repeated for individual amino acids, it was found that the mean pairwise backbone rmsd values between the free and complexed enzyme for Ala-7, Gly-9, and Ile-10 of β-strand A and for Asn-16 of turn I differed by more than two standard deviations over the sum of the rmsd values separately calculated for the free and complexed enzymes. Similarly, the mean pairwise rmsd values for all heavy atoms differed by more than two standard deviations for these same residues and also for Trp-90 and Trp-95 in loop III, indicating significant local conformational changes. These regions also show significant ^{15}N and NH backbone chemical shift changes (Lin *et al*., 1996) but not C_α or H_α chemical shift changes on binding Mg^{2+} and Mg^{2+}-AMPCPP. Changes in mean pairwise rmsd values smaller than two standard deviations, but above the sum of those found separately in the free and bound enzyme, occurred throughout the enzyme in regions which also showed changes in backbone ^{15}N and NH chemical shifts on binding Mg^{2+} and Mg^{2+}AMPCPP (Lin *et al*., 1996) and are predominantly at the sites of metal and substrate binding. As expected, the magnitudes of these smaller changes in structure did not correlate quantitatively with the chemical shift changes and may not be statistically significant. Hence, at the present level of refinement, changes in $^1H-^{15}N$ HSQC spectra provide more sensitive tests of conformational changes than can be resolved by a statistical comparison of the structures of free and complexed MutT.

Nucleotide Binding Site in the MutT−M^{2+}−AMPCPP−M^{2+} Complex: The Adenine−Ribose Subsite. AMPCPP is bound in a cleft formed by three of the five β-strands, A, C, and D, of the β-sheet on one side and the end of loop IV and the beginning of helix II on the other side (figure 5). Almost all amino acid side chains which approach the adenine−ribose moiety are hydrophobic such as Leu-4 and Ile-6 of β-strand A, Ile-80 and Leu-82 of β-strand D, and Tyr-73 and Phe-75 of β-strand C. The adenine ring interacts with a hydrophobic surface formed by Leu-4, Ile-6, and Ile-80. The plane of the adenine ring is perpendicular to those

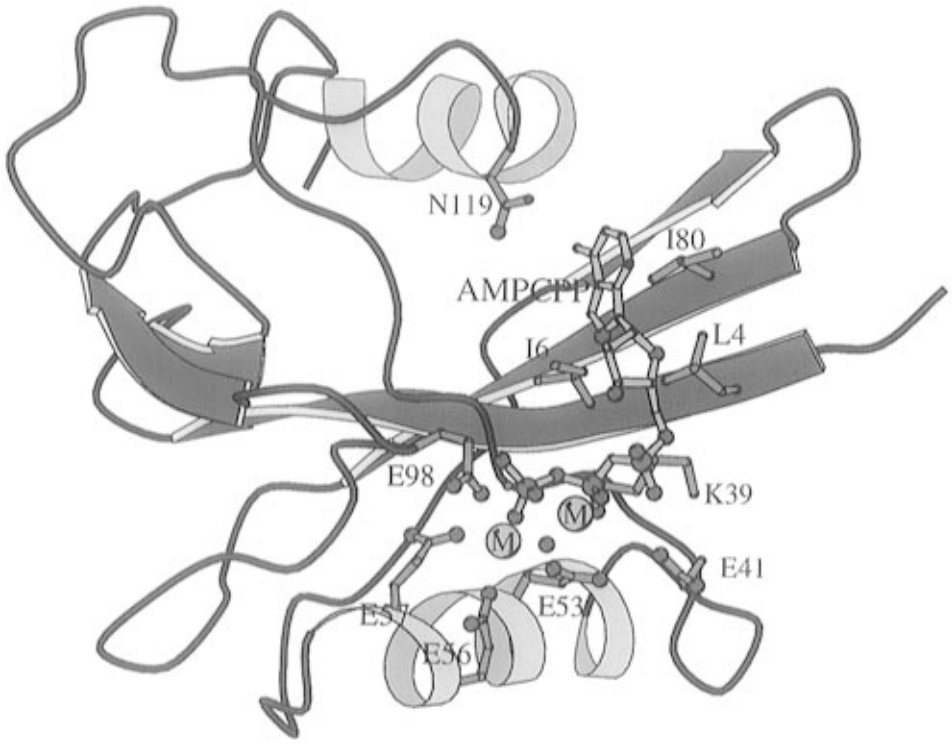

FIGURE 5: Structure of the lowest-energy quaternary complex which is most similar to the average structure in the active site region, showing the residues that interact with the enzyme-bound metal ion and with the metal−AMPCPP complex. The oxygen of the likely attacking water ligand on the enzyme-bound metal is also shown as a red sphere. This structure, drawn with MOLSCRIPT (Kraulis, 1991), shows backbone connectivities.

of Tyr-73 and Phe-75 located on β-strand C, with these two aromatic residues forming a pocket to hold the adenine ring.

On the other side of the cleft, the side chain amide NH_2 of Asn-119 closely approaches the 6-NH_2 group of AMPCPP (Figure 5) in all 16 acceptable structures, with a minimum interproton distance of 3.4 ± 0.5 Å averaged over the 16 acceptable structures. While this interproton distance exceeds the van der Waals sum of 2.4 Å by 1.0 ± 0.5 Å, electrostatic repulsion between these NH_2 groups may occur, contributing to the 4.2-fold higher K_M for adenine versus guanine nucleotides (Frick *et al*., 1995). With a keto group at the 6-position, guanine nucleotides would interact favorably with the NH_2 of Asn-119.

Two observations are consistent with the role of Asn-119 in substrate recognition by interacting with the 6-substituent of the purine ring. First, the side chain of Asn-119 is restricted by steric hindrance in a highly hydrophobic environment within 5 Å of Phe-35, Leu-71, Leu-82, Phe-84, and Ala-118. The aromatic rings of Phe-35 and Phe-84 may explain the unusually wide separation by 1.89 ppm of the two side chain NH chemical shifts of Asn-119 in HSQC spectra and the upfield chemical shift of the side chain ^{13}CO in CO(C)H spectra (174.72 ppm) in comparison with those of all of the other Asn residues of MutT which are in the range of 177.06−178.15 ppm. The binding of AMPCPP caused the chemical shift of the downfield NH proton of the side chain of Asn-119 to move upfield by 0.05 ppm, while the binding of dGTP caused the chemical shift of the downfield NH proton to move downfield, and by the greater amount of 0.54 ppm, suggesting that the side chain NH_2 of Asn-119 is involved in substrate recognition by forming a hydrogen bond with O_6 of the guanine ring and that it interacts differently with adenine, in which the O_6 is replaced by the 6-NH_2 group. Second, the ORF-17 enzyme, which catalyzes the same reaction as MutT and shows structural homology to MutT, but prefers dATP rather than dGTP as a substrate, has an Ala residue replacing Asn-119 (O'Handley *et al*., 1996).

Preferred substrates of the MutT enzyme have bulky substituents at C_8 of the purine ring such as 8-bromo-dNTP (Bhatnagar *et al*., 1991; Frick *et al*., 1995). The best substrate is the mutagenic nucleotide, 8-oxo-dGTP with a 2000-fold lower K_M than that of dGTP (Maki & Sekiguchi, 1994). Only hydrophobic residues such as Leu-4 and Ile-8 approach C_8 of bound AMPCPP, suggesting that van der Waals interactions with the substituent at C_8 may be responsible for the lower K_M of 8-oxo-dGTP. This optimum substrate of MutT is also protonated at N_7. However, only hydrophobic residues (Ile-6 and Leu-82) are near N_7 of bound AMPCPP, providing no additional explanation of the low K_M of 8-oxo-dGTP.

The hydrophobic face of the ribose ring of AMPCPP interacts with the side chains of Leu-4 and Ile-6 of β-strand A and with the δ-CH_2 of Lys-39 on loop I. The hydrophilic face of the sugar, bearing the two hydroxyl groups, is oriented toward the solvent.

Triphosphate Subsite and the Mechanism of the MutT Reaction. Kinetic studies with the substitution-inert $Co^{3+}(NH_3)_4ATP$ complex have previously shown that the MutT enzyme uses as substrate the β,γ-bidentate metal−ATP complex with the Λ configuration at P_β (Frick *et al*., 1994). Although the precise conformation of the Mg^{2+}−triphosphate moiety of bound Mg^{2+}AMPCPP is the least well defined structurally due to fewer distance restraints (Figure 6), its amino acid environment is not very sensitive to this variation. The side chain ammonium group of Lys-39 approaches an oxygen of the α-phosphoryl group at a distance of 4.7 ± 1.1 Å averaged over the 16 structures. It

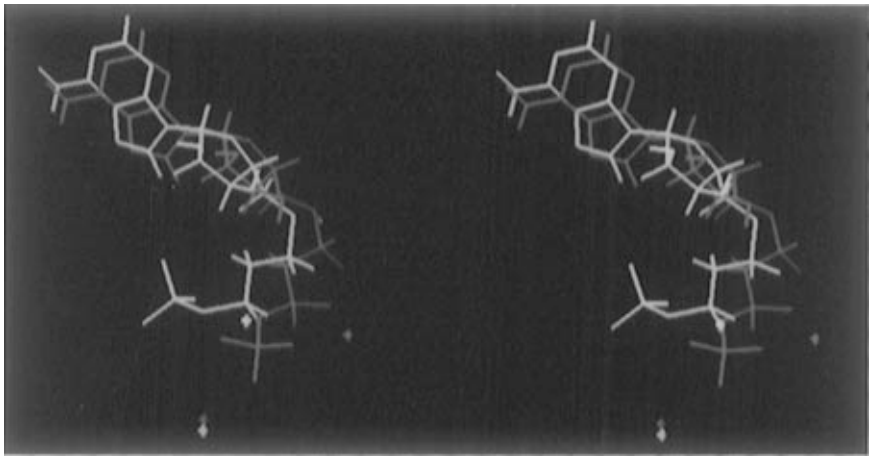

FIGURE 6: Stereopair of the two most different AMPCPP structures in the 16 acceptable MutT−M^{2+}−AMPCPP−M^{2+} complexes. All others lie between these two. The structures were aligned on all backbone heavy atoms of the MutT enzyme in the complex. The crosses at the bottom indicate the locations of the enzyme-bound metal ions, and the upper crosses are locations of the nucleotide-bound metal ions.

is somewhat farther from an oxygen of the β-phosphoryl group (6.0 ± 0.7Å) and farthest from an oxygen of the γ-phosphoryl group (8.9 ± 0.7Å) (Figure 7). These results suggest that Lys-39 activates the leaving NMP group by electrostatic interaction. Mutation of Lys-39 to Gln results in an 8-fold decrease in k_{cat} and a 5.3-fold increase in K_M (dGTP) in the Mg^{2+}-activated dGTPase reaction (Frick *et al*., 1995).

The triphosphate extends across loop I near the conserved residues Gly-38 and Glu-98, approaches the cluster of conserved Glu residues from helix I, and forms a second sphere complex of the enzyme-bound divalent cation (Figures 5 and 7). The position of the enzyme-bound divalent cation is fixed by the ligands, Glu-56, -57, and -98, and the carbonyl group of Gly-38 (Figure 8). A residue larger than the conserved Gly at position 38 would disrupt the coordination sphere of the enzyme-bound metal by colliding with the carboxylate of Glu-98.

The octahedral coordination of the enzyme-bound metal is completed by two water ligands, one of which closely approaches the reaction center β-phosphorus with a P_β−OH_2 distance of 4.2 ± 0.2 Å averaged over the 16 structures. This short reaction coordinate distance is consistent with an associative nucleophilic substitution at P_β by water since it is significantly less than the limiting value of 4.9 Å which is required to provide enough room for a metaphosphate type intermediate in a dissociative mechanism (Mildvan, 1981). As with phosphodiesters (Weber *et al*., 1992b), an associative mechanism of substitution at P_β of an NTP is much more likely than a dissociative one (Mildvan & Fry, 1987). The oxygen of this water ligand on MutT may be close enough to the two carboxylate oxygens of Glu-53 (2.6 ± 0.2 and 3.6 ± 0.4Å) to donate a hydrogen bond to at least one of them, suggesting either general base catalysis or orientation of the attacking water (or hydroxyl) ligand by Glu-53. The angle of attack, defined by the water oxygen, the attacked P_β, and the "leaving" methylene carbon, averaged over the 16 structures, is 126 ± 11°, differing from the ideal value of 180° which is expected for a single displacement at phosphorus with inversion. While the stereochemistry of the MutT reaction has not been determined, staphylococcal nuclease, which has a very similar reaction coordinate distance of 4.3 Å between a Ca^{2+}-bound water ligand and the substrate phosphorus, and a similar angle of attack of 131 ± 16° (Weber *et al*., 1992b), shows stereochemical inversion at phosphorus (Mehdi & Gerlt, 1982).

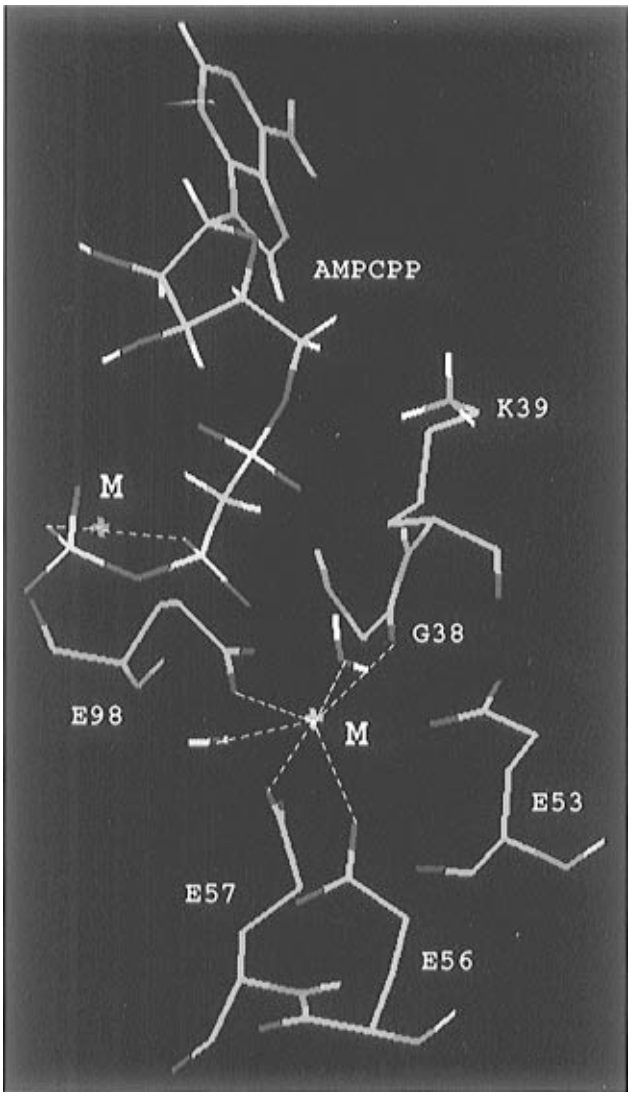

FIGURE 7: Reaction center of the MutT enzyme from the lowest-energy structure of the quaternary complex, showing residues and water molecules that interact with the enzyme-bound metal and the triphosphate group of M^{2+}−AMPCPP. The water ligand, *cis* to Gly-38 and near both Pβ and Glu-53, is well positioned to be the attacking nucleophile.

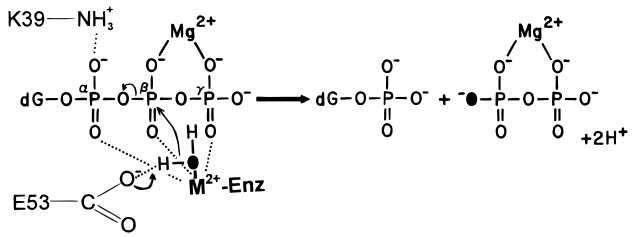

FIGURE 8: Mechanism of the MutT reaction consistent with the structure of the quaternary E−M^{2+}−NTP−M^{2+} complex and with kinetic data (Frick *et al*., 1994, 1995) showing possible roles for Lys-39 and Glu-53. Alternatively, Glu-53 may function solely to orient the attacking nucleophile. For clarity, the enzyme-bound divalent cation is depicted as M^{2+}, and the nucleotide-bound divalent cation is depicted as Mg^{2+}.

A search of the 16 structures revealed no nucleophilic residues at the active site of MutT which might attack P_β as part of a double-displacement mechanism. The four nearest residues to P_β are Lys-39, Glu-41, Glu-53, and Glu-98 with average P_β−N_ζ or P_β−O_δ distances of 6.0 ± 0.7, 5.9 ± 0.8, 6.2 ± 0.3, and 4.6 ± 0.9 Å, respectively. The reaction coordinate distances of Lys-39, Glu-41, and Glu-53 are significantly greater than the 4.9 Å limit expected for an associative mechanism. Moreover, a much larger decrease in k_{cat} than 8-fold would be expected in the K39Q mutant if Lys-39 were an essential nucleophile, and Glu-41 is not conserved among MutT like enzymes. While the P_β−O distance for Glu-98 is appropriate for an associative mechanism, Glu-98 is a ligand to the enzyme-bound divalent cation and therefore cannot function as a nucleophile. All other potential nucleophilic residues are more than 8 Å from P_β. Hence, a single displacement at P_β by water, as previously suggested (Weber *et al*., 1992a), is much more likely than a double displacement.

While the positions of the backbone atoms of the solvent-exposed and highly conserved residue Arg-52 are well determined in the middle of helix I by 19 NOEs involving backbone resonances, the orientation of the side chain is not well defined in the free enzyme (Figure 1) or in the quaternary complex. Systematic variation of the side chain orientation with the program CHAIN reveals that the guanidinium remains at least 8 Å from the triphosphate of bound AMPCPP in the quaternary complex, indicating that Arg-52 cannot interact directly with the substrate. However, the guanidinium can approach a carboxylate oxygen of Glu-53 to within hydrogen bonding distance, suggesting that Arg-52 may orient Glu-53, which in turn orients the attacking water. Mutation of Arg-52 to Gln results in at least a 10^2-fold loss of MutT activity as estimated by both *in vitro* dGTPase assays (Frick *et al*., 1995) and *in vivo* complementation of a mutT deficient strain of *Escherichia coli*.[3]

A mechanism of the MutT reaction consistent with the solution structure of the quaternary enzyme−M^{2+}−AMPCPP−M^{2+} complex (Figure 8) thus involves direct nucleophilic attack on the β-phosphorus of the M^{2+}−NTP substrate by a water or hydroxyl ligand of the enzyme-bound divalent cation, assisted by the nucleotide-bound divalent cation which neutralizes charge at the β-phosphoryl group, by Glu-53 functioning either as a general base or to orient the attacking nucleophile and by Lys-39 which promotes the departure of the leaving group.

[3] D. N. Frick, unpublished observations, 1995.

Quantitatively, the MutT enzyme with a k_{cat} value of 4.0 s^{-1} (Frick *et al*., 1994) accelerates the rate of nucleophilic substitution at the electron-rich β-phosphorus of NTP substrates by a factor of 10^9 in comparison with the rates of model reactions extrapolated to the same temperature and pH (Van Wazer *et al*., 1955). A major contribution of at least 10^5-fold to the catalytic power of MutT is provided by the enzyme-bound divalent cation which presents the attacking water or hydroxyl nucleophile to P_β, thus promoting catalysis by approximation. The factor of $\geq 10^5$ is suggested by the observation that mutation of the liganding residue Glu-57 to Gln weakened metal binding by 3.5-fold but decreased catalytic activity by at least 10^5-fold due in part to an altered position of the enzyme-bound divalent cation (Lin *et al*., 1996). Assuming additivity of effects (Mildvan *et al*., 1992), another factor of ~10 in catalytic power may be provided by Lys-39 as suggested by the effect of the K39Q mutation on k_{cat} (Frick *et al*., 1995). The nucleotide-bound divalent cation contributes at least 1 order of magnitude by charge neutralization at P_β as suggested by the 20-fold decrease in activity on replacing Mg^{2+} at this position with Co^{3+} (Frick *et al*., 1994). The remaining factor of $\leq 10^2$ may be provided by Glu-53 which either deprotonates or orients the attacking water and which in turn may be oriented by Arg-52, in accord with the $\geq 10^2$-fold loss of activity of the R52Q mutant (Frick *et al*., 1995).[3] Although this point has not yet been tested directly by mutagenesis of Glu-53, general base catalysis has been shown in other enzymes to contribute factors ranging from 10^2 to 10^6 to catalysis (Mildvan *et al*., 1992, and references therein). Clearly, additional single and multiple mutations will be necessary to further test these contributions and their additivities.

It is of interest to note that all enzymes that catalyze nucleophilic substitution at the electron-rich β-phosphorus of NTP substrates appear to require two divalent cations (Frick *et al*., 1994) and show comparably low catalytic powers, with k_{cat} values ranging from 0.3 to 10 s^{-1} (Kaziro, 1959; Talarico *et al*., 1992). While MutT represents the first structure of an enzyme of this class, another such enzyme, phosphoribosyl pyrophosphate synthetase, is also known to form a second sphere complex between the enzyme-bound divalent cation and the metal−nucleotide substrate (Granot *et al*., 1980a). Hence, mechanisms similar to that of Figure 8 may apply to other pyrophosphotransferases as well.

CONCLUSIONS

As determined by solution NMR methods, the binding of the essential divalent cation activator Mg^{2+} and the substrate analog Mg^{2+}AMPCPP to the MutT enzyme to form the quaternary E−Mg^{2+}−AMPCPP−Mg^{2+} complex does not alter the global fold of the enzyme but produces localized, small conformational changes at or near the metal and substrate binding sites. The adenine−ribose moiety binds in a hydrophobic cleft near three strands of a mixed β-sheet, with the 6-NH_2 group of the purine ring approaching the NH_2 side chain of Asn-119. With a 6-keto group, GTP would interact more favorably with Asn-119, consistent with the substrate preference of MutT for guanine over adenine nucleotides. The enzyme-bound metal is coordinated by three conserved Glu residues (56, 57, and 98), by the backbone carbonyl of a conserved Gly residue (38), and by two water ligands. The metal−triphosphate moiety of the metal−AMPCPP complex appears to bind in the second

coordination sphere of the enzyme-bound divalent cation. One of the water ligands of the enzyme-bound metal ion is well positioned to attack P_β with inversion and to be deprotonated or oriented by Glu-53. Lys-39 is positioned to interact electrostatically with the α-phosphoryl group and thereby to facilitate the departure of the NMP leaving group. This reaction mechanism, derived from the solution structure of the quaternary MutT complex, is qualitatively and quantitatively consistent with the results of mutagenesis and kinetic studies and may well be applicable to other enzymes which catalyze nucleophilic substitution at the electron-rich P_β of NTP substrates.

ACKNOWLEDGMENT

We are grateful to Joel R. Gillespie for help in the preparation of $Co^{3+}(NH_3)_4$AMPCPP and to Apostolos Gittis and Frithjof Kuntze for assistance in preparing Figure 4.

SUPPORTING INFORMATION AVAILABLE

One table containing the ^1H, ^{13}C, and ^{15}N chemical shifts of the MutT protein in MutT−Mg^{2+}−AMPCPP−Mg^{2+} from *E. coli* and one table containing the side chain $^{13}C{=}O$ chemical shifts of the free enzyme (10 pages). Ordering information is given on any current masthead page.

REFERENCES

Abeygunawardana, C., Weber, D. J., Frick, D. N., Bessman, M. J., & Mildvan, A. S. (1993) *Biochemistry 32*, 13071−13080.

Abeygunawardana, C., Weber, D. J., Gittis, A. G., Frick, D. N., Miller, A.-F., Bessman, M. J., Lin, J., & Mildvan, A. S. (1995) *Biochemistry 34,* 14997−15005.

Abeygunawardana, C., Mori, S., Van Zihl, P. C. M., & Mildvan, A. S. (1996) *34th Experimental NMR Conference*, Pacific Grove, CA, abstract WP4, p 224, ENC Publications, Santa Fe, NM.

Bax, A., Clore, G. M., & Gronenborn, A. M. (1990) *J. Magn. Reson. 88*, 425−431.

Bessman, M. J., Frick, D. N., & O'Handley, S. F. (1996) *J. Biol. Chem. 271*, 25059−25066.

Bhatnagar, S. K., Bullions, L. C., & Bessman, M. J. (1991) *J. Biol. Chem. 266*, 9050−9054.

Bodenhausen, G., & Ruben, D. J. (1980) *Chem. Phys. Lett. 69*, 185−188.

Brooks, R. R., Bruccoleri, R. E., Olafson, B. D., States, D. J., Swaminathan, S., & Karplus, M. J. (1983) *J. Comput. Chem. 4*, 187−217.

Brünger, A. T. (1992) *X-PLOR Version 3.1. A system for X-ray crystallography and NMR*, Yale University Press, New Haven, CT.

Cheng, K. C., Cahill, D. S., Kasai, H., Nishimura, S., & Loeb, L. A. (1991) *J. Biol. Chem. 267*, 166−172.

Cleland, W. W., & Mildvan, A. S. (1979) in *Advances in Inorganic Biochemistry* (Eichorn, G. L., & Marzilli, L.,Eds.) Vol. 1, pp 163−191, Elsevier, New York.

Clore, G. M., Nilges, M., Sukumaran, D. K., Brünger, A. T., Karplus, M., & Gronenborn, A. M. (1986) *EMBO 5*, 2729−2735.

Clore, G. M., Gronenborn, A. M., Nilges, M., & Ryan, C. A. (1987) *Biochemistry 26*, 8012−8013.

Cornelius, R. D., Hart, P. A., & Cleland, W. W. (1977) *Inorg. Chem. 16*, 2799−2805.

Frick, D. N., Weber, D. J., Gillespie, J. R., Bessman, M. J., & Mildvan, A. S. (1994) *J. Biol. Chem. 269*, 1794−1803.

Frick, D. N., Weber, D. J., Abeygunawardana, C., Gittis, A. G., Bessman, M. J., & Mildvan, A. S. (1995) *Biochemistry 34*, 5577−5586.

Granot, J., Gibson, K. J., Switzer, R. L., & Mildvan, A. S. (1980a) *J. Biol. Chem. 255*, 10931−10937.

Granot, J., Mildvan, A. S., Bramson, H. N., & Kaiser, E. T. (1980b) *Biochemistry 19*, 3537−3543.

Kakuma, T., Nishida, J., Tsuzuki, T., & Sekiguchi, M. (1995) *J. Biol. Chem. 270*, 25942−25948.

Kay, L. E. (1993) *J. Am. Chem. Soc. 115*, 2055−2057.

Kay, L. E., & Bax, A. (1990) *J. Magn. Reson. 86*, 110−126.

Kay, L. E., Xu, G.-Y., Singer, A. U., Muhandiram, D. R., & Forman-Kay, J. D. (1993) *J. Magn. Reson. 101B*, 333−337.

Kaziro, Y. (1956) *J. Biochem. (Tokyo) 46,* 1523−1539.

Kraulis, P. J. (1991) *J. Appl. Crystallogr. 24*, 946−950.

Lee, W., Revington, M. J., Arrowsmith, C., & Kay, L. E. (1994) *FEBS Lett. 350,* 87−90.

Lee, W., Revington, M., Farrow, N. A., Nakamura, A., Utsunomiya-Tate, N., Miyake, Y., Kainosho, M., & Arrowsmith, C. H. (1995) *J. Biomol. NMR 5,* 367−375.

Levy, G. C., & Lichter, R. L. (1979) *Nitrogen-15 Nuclear Magnetic Resonance Spectroscopy*, John Wiley & Sons, New York.

Lin, J., Abeygunawardana, C., Frick, D. N., Bessman, M. J., & Mildvan, A. S. (1996) *Biochemistry 35*, 6715−6726.

Maki, H., & Sekiguchi, M. (1992) *Nature 355*, 273−275.

Marion, D., & Wüthrich, K. (1983) *Biochem. Biophys. Res. Commun. 113*, 967−974.

Marion, D., Ikura, M., Tschudin, R., & Bax, A. (1989) *J. Magn. Reson. 85*, 393−399.

Mehdi, S., & Gerlt, J. A. (1982) *J. Am. Chem. Soc. 104*, 3223−3225.

Mildvan, A. S. (1981) *Philos. Trans. R. Soc. London Ser. B 293*, 65−74.

Mildvan, A. S., & Gupta, R. K. (1978) *Methods Enzymol. 49G*, 322−359.

Mildvan, A. S., & Fry, D. C. (1987) *Adv. Enzymol. 59*, 241−313.

Mildvan, A. S., Weber, D. J., & Kuliopulos, A. (1992) *Arch. Biochem. Biophys. 294*, 327−340.

Mo, J. Y., Maki, H., & Sekiguchi, M. (1992) *Proc. Natl. Acad. Sci. U.S.A. 89*, 11021−11025.

Mori, S., Abeygunawardana, C., Johnson, M. O., & van Zijl, P. C. M. (1995) *J. Magn. Reson. 108B*, 94−98.

Muhandiram, D. R., Farrow, N. A., Xu, G.-Y., Smallcombe, S. H., & Kay, L. E. (1993) *J. Magn. Reson. 102B*, 317−321.

Nilges, M., Clore, G. M., & Gronenborn, A. M. (1988) *FEBS Lett. 229*, 317−324.

O'Handley, S. F., Frick, D. N., Bullions, L. C., Mildvan, A. S., & Bessman, M. J. (1996) *J. Biol. Chem. 271*, 24649−24654.

Sakumi, K., Furuichi, M., Tsuzuki, T., Kakuma, T., Kawabata, S., Maki, H., & Sekiguchi, M. (1993) *J. Biol. Chem. 268*, 23524−23530.

Serpersu, E. H., McCracken, J., Peisach, J., & Mildvan, A. S. (1988) *Biochemistry 27*, 8034−8044.

Talarico, T. L., Ray, P. H., Dev, I. K., Merrill, B. M., & Dallas, W. S. (1992) *J. Bacteriol. 174*, 5971−5977.

Van Wazer, J. R., Griffith, E. J., & McCullough, J. F. (1955) *J. Am. Chem. Soc. 77*, 287−291.

Villafranca, J. J., & Mildvan, A. S. (1972) *J. Biol. Chem. 247*, 3454−3463.

Vuister, G. W., & Bax, A. (1992) *J. Magn. Reson. 98*, 428−435.

Weber, D. J., Mullen, G. P., & Mildvan, A. S. (1991) *Biochemistry 30*, 7425−7437.

Weber, D. J., Bhatnagar, S. K., Bullions, L. C., Bessman, M. J., & Mildvan, A. S. (1992a) *J. Biol. Chem. 267*, 16939−16942.

Weber, D. J., Gittis, A. G., Mullen, G. P., Abeygunawardana, C., Lattman, E. E., & Mildvan, A. S. (1992b) *Proteins: Struct., Funct., Genet. 13*, 275−287.

Weber, D. J., Abeygunawardana, C., Bessman, M. J., & Mildvan, A. S. (1993) *Biochemistry 32*, 13081−13088.

Wüthrich, K. (1986) *NMR of Proteins and Nucleic Acids*, pp 166−168, John Wiley & Sons, New York.

Wüthrich, K., Billetter, M., & Braun, W. (1983) *J. Mol. Biol. 169*, 949−961.

Yanofsky, C., Cox, E. C., & Horn, V. (1966) *Proc. Natl. Acad. Sci. U.S.A. 55*, 274−281.

BI962619C